BIOCHEMISTRY
including biophysical chemistry & molecular biology

Article

pubs.acs.org/biochemistry

Participation of Glutamate-333 of the D1 Polypeptide in the Ligation of the Mn_4CaO_5 Cluster in Photosystem II

Rachel J. Service,[†,⊥] Junko Yano,[‡] Preston L. Dilbeck,[§,#] Robert L. Burnap,[§] Warwick Hillier,[¶] and Richard J. Debus*[,†]

[†]Department of Biochemistry, University of California, Riverside California 92521, United States

[‡]Physical Biosciences Division, Lawrence Berkeley National Laboratory, Berkeley, California 94720, United States

[§]Department of Microbiology and Molecular Genetics, Oklahoma State University, Stillwater, Oklahoma 74078, United States

[¶]Research School of Biology, The Australian National University, Canberra, Australian Capital Territory 0200, Australia

ABSTRACT: In the 1.9 Å structural model of photosystem II (PDB: 3ARC), the amino acid residue Glu333 of the D1 polypeptide coordinates to the oxygen-evolving Mn_4CaO_5 cluster. This residue appears to be highly significant in that it bridges the two Mn ions (Mn_{B3} and the "dangling" Mn_{A4}) that are also bridged by the oxygen atom O5. This oxygen atom has been proposed to be derived from one of two substrate water molecules and to become incorporated into the product dioxygen molecule during the final step in the catalytic cycle. In addition, the backbone nitrogen of D1-Glu333 interacts directly with a nearby Cl^- atom. To further explore the influence of this structurally unique residue on the properties of the Mn_4CaO_5 cluster, the D1-E333Q mutant of the cyanobacterium *Synechocystis sp.* PCC 6803 was characterized with a variety of biophysical and spectroscopic methods, including polarography, EPR, X-ray absorption, and FTIR difference spectroscopy. The kinetics of oxygen release in the mutant were essentially unchanged from those in wild-type. In addition, the oxygen flash yields exhibited normal period-four oscillations having normal S state parameters, although the yields were lower, indicative of the mutant's lower steady-state dioxygen evolution rate of approximately 30% compared to that of the wild-type. The S_1 state Mn-XANES and Mn-EXAFS and S_2 state multiline EPR signals of purified D1-E333Q PSII core complexes closely resembled those of wild-type, aside from having lower amplitudes. The S_{n+1}-*minus*-S_n FTIR difference spectra showed only minor alterations to the carbonyl, amide, and carboxylate stretching regions. However, the mutation eliminated a negative peak at 3663 cm^{-1} in the weakly H-bonding O—H stretching region of the S_2-*minus*-S_1 FTIR difference spectrum and caused an approximately 9 cm^{-1} downshift of the negative feature in this region of the S_1-*minus*-S_0 FTIR difference spectrum. We conclude that fully functional Mn_4CaO_5 clusters assemble in the presence of the D1-E333Q mutation but that the mutation decreases the yield of assembled clusters and alters the H-bonding properties of one or more water molecules or hydroxide groups that are located on or near the Mn_4CaO_5 cluster and that either deprotonate or form stronger hydrogen bonds during the S_0 to S_1 and S_1 to S_2 transitions.

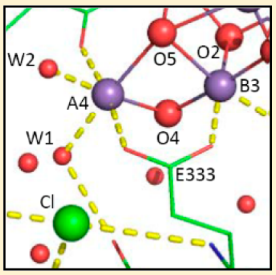

The light-driven oxidation of water in photosystem II (PSII) [see Abbreviations] produces nearly all of the O_2 on Earth and drives the production of nearly all of its biomass. Photosystem II is an integral membrane protein complex that is located in the thylakoid membranes of plants, algae, and cyanobacteria.[1−4] It is a homodimer in vivo, having a total molecular weight of approximately 700 kDa with each monomer containing at least 20 different subunits and nearly 60 organic and inorganic cofactors including 35 Chl *a*, 11 carotenoid, 2 pheophytin, and 2 plastoquinone molecules. The O_2-evolving catalytic center in PSII consists of a Mn_4CaO_5 cluster and its immediate protein environment. In response to photochemical events within PSII, the Mn_4CaO_5 cluster accumulates four oxidizing equivalents and then catalyzes the oxidation of two molecules of water, releasing one molecule of O_2 as a byproduct.[5−9] The Mn_4CaO_5 cluster serves as the interface between single-electron photochemistry and the four-electron process of water oxidation. The photochemical events that precede water oxidation take place in a heterodimer of two homologous 38−39 kDa polypeptides known as D1 and D2. These events are initiated by the transfer of excitation energy to the photochemically active Chl *a* multimer known as P_{680} following the capture of light energy by the antenna complex. Excitation of P_{680} results in the formation of the charge-separated state, $P_{680}^{\bullet+}Pheo^{\bullet-}$. This light-induced separation of charge is stabilized by the rapid oxidation of $Pheo^{\bullet-}$ by Q_A, the primary plastoquinone electron acceptor, and by the rapid reduction of $P_{680}^{\bullet+}$ by Y_Z, one of two redox-active tyrosine residues in PSII. The resulting $Y_Z^{\bullet}$ radical in turn oxidizes the Mn_4CaO_5 cluster, whereas $Q_A^{\bullet-}$ reduces the secondary plastoquinone, Q_B. Subsequent charge-separations result in further oxidation of the Mn_4CaO_5 cluster and in the two-electron reduction and protonation of Q_B to form plastoquinol, which subsequently exchanges into the membrane-bound plastoquinone pool. During each catalytic cycle, the

Received: September 29, 2013
Revised: October 29, 2013
Published: October 29, 2013

dx.doi.org/10.1021/bi401339f | *Biochemistry* 2013, 52, 8452−8464

Mn_4CaO_5 cluster advances through five oxidation states termed S_n, where n denotes the number of oxidizing equivalents that are stored ($n = 0 - 4$). The S_1 state predominates in dark-adapted samples. The S_4 state is a transient intermediate whose formation triggers the formation and release of O_2 and the regeneration of the S_0 state.

In the recent 1.9 Å crystallographic structural model of PSII (PDB: 3ARC)[1,10] and in subsequent computational refinements of the structure of the Mn_4CaO_5 cluster and its ligation environment,[11−16] three Mn ions (Mn_{D1}, Mn_{C2}, and Mn_{B3} [we have adopted the combined crystal structure and EPR-based notation for the Mn ions advanced in refs 8 and 9]), the Ca ion, and four oxygen bridging ligands (O1, O2, O3, and O5) form a distorted cube that is linked to a fourth "dangling" Mn ion (Mn_{A4}) by O5 and by an additional oxygen bridging ligand (O4). In these models, Glu333 of the D1 polypeptide is a bidentate bridging ligand of the Mn_4CaO_5 cluster, coordinating to both Mn_{B3} and Mn_{A4} (Figure 1). In recent proposals for the mechanism of O−O bond formation, O5 derives from one of the two substrate water molecules and becomes incorporated into the product dioxygen molecule by reacting with another substrate water-derived Mn or Ca ligand.[8,9,17−22] Recent pulsed EPR studies[20,22] have provided support for these proposals by providing strong evidence that O5 corresponds to the slowly exchanging substrate water molecule. Structural flexibility of the Mn_4CaO_5 cluster is a key aspect of these proposals, and there is an emerging consensus that the Mn_4CaO_5 cluster readily interconverts between two nearly isoenergetic conformers during the S state cycle, with O5 ligating Mn_{A4} in one conformer (giving rise to the multiline EPR signal in the S_2 state) and ligating Mn_{D1} in the other (giving rise to the $g = 4.1$ EPR signal in the S_2 state).[8,9,16,23] In the S_2 state, this interconversion is linked to a redox isomerization, with the Mn ion *not* binding O5 being in its Mn(III) oxidation state in addition to having an open coordination position along its Jahn−Teller axis. A similar structural conversion involving changes in the ligation of O5 during the S_2 to S_3 transition has also been proposed on the basis of a recent Mn-EXAFS study.[24] Consequently, the carboxylate group of D1-Glu333 coordinates to a particularly dynamic region of the Mn_4CaO_5 cluster in its most solvent-accessible domain, linking the cuboidal Mn_3CaO_4 unit with the dangling Mn ion, ligating a Mn ion (Mn_{A4}) whose coordination number may change during the catalytic cycle, and sharing two Mn ions (Mn_{A4} and Mn_{B3}) with O5. In addition, the backbone nitrogen of D1-Glu333 interacts directly with the Cl^- ion that is ligated by D2-Lys317. This residue has been proposed[25,26] to participate in a network of hydrogen bonds that facilitates the deprotonation reactions that are required for oxidizing the Mn_4CaO_5 cluster in its higher oxidation states.[27−31]

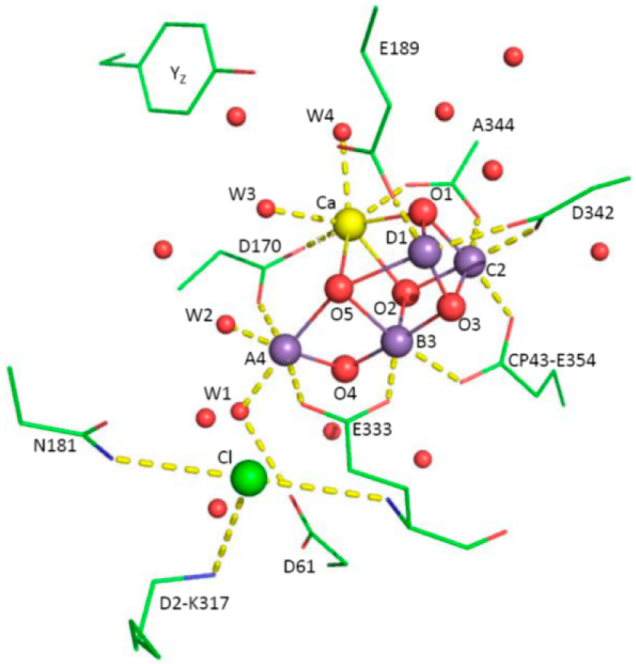

Figure 1. Mn_4CaO_5 cluster and its environment[1] showing the position of D1-Glu333 in relation to Mn_{A4}, Mn_{B3}, and the Cl^- ion that is ligated by D2-Lys317. For clarity, only selected residues are shown. Except as noted otherwise, all residues are from the D1 polypeptide. Purple spheres, manganese ions [the labels A4, B3, C2, and D1 reflect the combined crystal structure and EPR-based notations for the Mn ions advanced in refs 8 and 9]; yellow sphere, calcium; large red spheres, μ-oxo bridges; green sphere, chloride; small red spheres, water molecules including the four water molecules bound to Mn_{A4} (W1 and W2) and Ca (W3 and W4).

Of all the mutations reported to have been constructed at D1-Glu333 (Gln, Asp, Asn, His, Cys, Ala, and Tyr), only the D1-E333Q mutation supports the photoautotrophic propagation of cells, and this only in dim light.[32−34] When propagated in dim light, the PSII content of D1-E333Q cells is 58−65% compared to that of wild-type cells. Under continuous illumination under light-saturating conditions, D1-E333Q cells evolve O_2 at approximately 30% of the rate of wild-type cells. To further explore the influence of this structurally unique residue on the properties of the Mn_4CaO_5 cluster, we have characterized the D1-E333Q mutant of the cyanobacterium *Synechocystis sp.* PCC 6803 with a variety of biophysical and spectroscopic methods, including polarography, EPR, Mn-XANES, Mn-EXAFS, and FTIR difference spectroscopy. We conclude that fully functional Mn_4CaO_5 clusters assemble in the presence of the D1-E333Q mutation but that the mutation decreases the yield of assembled clusters and alters the H-bonding properties of one or more water molecules or hydroxide groups that are located on or near the Mn_4CaO_5 cluster and that either deprotonate or form stronger hydrogen bonds during the S_0 to S_1 and S_1 to S_2 transitions.

MATERIALS AND METHODS

Construction of Mutant and Propagation of Cultures.

The D1-E333Q mutation was constructed in the *psbA-2* gene of *Synechocystis sp.* PCC 6803[35] and transformed into a host strain of *Synechocystis* that lacks all three *psbA* genes and contains a hexahistidine-tag (His-tag) fused to the C-terminus of CP47.[36] Single colonies were selected for their ability to grow on solid media containing 5 μg/mL kanamycin monosulfate. Solid media contained 5 mM glucose and 10 μM DCMU. The DCMU and antibiotic were omitted from the liquid cultures. Large-scale liquid cultures (each consisting of three 7 L cultures held in glass carboys) were propagated as described previously.[37] To verify the integrity of the mutant cultures that were harvested for the purification of thylakoid membranes and PSII core complexes, an aliquot of each culture was set aside and the sequence of the relevant portion of the *psbA-2* gene was obtained after PCR amplification of genomic DNA.[35] No trace of the wild-type codon was detected in any of the mutant cultures.

dx.doi.org/10.1021/bi401339f | *Biochemistry* 2013, 52, 8452−8464

Purification of Thylakoid Membranes. Thylakoid membranes were isolated under dim green light at 4 °C with a procedure[38] modified from that of Tang and Diner.[39] Harvested cells were concentrated and suspended in a buffer containing 1.2 M betaine, 10% (v/v) glycerol, 50 mM MES−NaOH (pH 6.0), 5 mM $CaCl_2$, 5 mM $MgCl_2$, 1 mM benzamidine, 1 mM ε-amino-n-caproic acid, 1 mM phenymethylsulfonyl fluoride, and 0.05 mg/mL DNase I and then broken by nine cycles of 5 s on/15 min off in a glass bead homogenizer (Bead-Beater, BioSpec Products, Bartlesville, OK) [The use of betaine was suggested to us by ref 40]. After separation of unbroken cells and debris by low speed centrifugation, the resulting thylakoid membranes were concentrated by ultracentrifugation (20 min at 40 000 rpm in a Beckman Ti45 rotor) and suspended to a concentration of 1.0−1.5 mg of Chl/mL in TM buffer [1.2 M betaine, 10% (v/v) glycerol, 50 mM MES−NaOH (pH 6.0), 20 mM $CaCl_2$, 5 mM $MgCl_2$]. The concentrated thylakoid membranes were either flash frozen as 1 mL aliquots in liquid nitrogen and stored at −80 °C or used immediately for the purification of PSII core complexes.

Purification of PSII Core Complexes. Oxygen-evolving PSII core complexes were purified under dim green light at 4 °C as described previously.[38] To a suspension of freshly prepared thylakoid membranes (60 − 100 mg of Chl), the detergent *n*-dodecyl-β-D-maltoside (Anatrace Inc., Maumee, OH) was added dropwise with gentle stirring from a stock of 10% (w/v) detergent (dissolved in TM buffer) to final concentrations of 1 mg of Chl/mL and 1% (w/v) detergent.[39] Extraction was allowed to proceed with gentle stirring for an additional 10 min in darkness. Unsolubilized material was pelleted by centrifuging at 17 500 rpm in a Beckman JA-20 rotor for 10 min.[41] The supernatant was loaded at a flow rate of 2.5 mL/min onto 40 mL of Ni-NTA superflow affinity resin (Qiagen Inc., Valencia, CA) that had been packed in a 5 cm diameter chromatography column and equilibrated with PSII buffer [1.2 M betaine, 10% (v/v) glycerol, 50 mM MES−NaOH (pH 6.0), 20 mM $CaCl_2$, 5 mM $MgCl_2$, 0.03% (w/v) *n*-dodecyl-β-D-maltoside]. After loading, the column was washed with four bed volumes of PSII buffer at a flow rate of 5 mL/min and then eluted with four bed volumes of PSII buffer containing 50 mM histidine. The eluent was brought to 1 mM EDTA and concentrated by ultrafiltration [Amicon Models 2000 and 8400 fitted with YM-100 membranes, followed by Amicon Ultra-4 100 K centrifugal filter devices (EMD Millipore, Billerica, MA)] to approximately 1 mg of Chl/mL. The purified PSII core complexes [in 1.2 M betaine, 10% (v/v) glycerol, 50 mM MES−NaOH (pH 6.0), 20 mM $CaCl_2$, 5 mM $MgCl_2$, 50 mM histidine, 1 mM EDTA, and 0.03% (w/v) *n*-dodecyl-β-D-maltoside] were aliquotted, frozen in liquid N_2, and stored at −196 °C (vapor phase nitrogen).

Flash O_2 Yield and Kinetic Measurements. Measurements were performed with a bare platinum electrode that permits the centrifugal deposition of samples onto the electrode surface.[42,43] Before deposition, thylakoid membranes were concentrated by centrifugation and suspended at ∼0.8 mg of Chl/mL in 50 mM HEPES−NaOH (pH 7.2), 200 mM NaCl, 5 mM $CaCl_2$, 10 mM $MgCl_2$, and 1 M sucrose.[44] For determination of the S-state cycling parameters estimated from the oscillatory patterns of O_2 release by dark adapted PSII, thylakoid membrane samples containing 3.2 μg of Chl were deposited on the platinum surface of the platinum electrode, exposed to room light for 30 s, and then centrifuged at 18 000*g* for 10 min in a Sorvall HB-4 swing-out rotor. Samples were given a single preflash and then dark adapted for 10 min prior to the initiation of the measuring flash sequence. Flashes were provided by a xenon flash lamp (6 μs fwhm). The treatment with room light was applied to oxidize PSII centers that may populate the "super-reduced" S_{-1} and S_{-2} states. The 10 min dark-adaptation period was incorporated to allow PSII centers to relax to the S_1 and S_0 states. Polarization of the electrode (0.73 V) was initiated 10 s before the initiation of data acquisition and the measuring flash sequence (19 flashes at a frequency of 4 Hz) was initiated 333 ms after that. Numerical extraction of the S state parameters was performed assuming a four-state model.[45,46] To measure the kinetics of O_2 release, samples were prepared as above, except that a light-emitting diode (Luxeon, Phillips) delivering a 30 microsecond pulse of 627 nm light was used instead of a xenon flash lamp to minimize the extent of the flash artifact as described previously.[44] The kinetics of O_2 release were estimated from the rising portion of the O_2 signal using the exponential method.[47]

Preparation of EPR and X-ray Absorption Samples. Samples for EPR measurements were concentrated to 7−8 mg of Chl/mL with Amicon Ultra-4 100 K centrifugal filter devices (EMD Millipore, Billerica, MA), transferred into standard quartz 4 mm o.d. EPR tubes (Wilmad LabGlass, Buena, NJ), dark adapted for 3 h at 4 °C, and then frozen in liquid nitrogen. Samples for X-ray absorption studies were transferred to a buffer containing 1.2 M betaine, 40% (v/v) glycerol, 50 mM MES−NaOH (pH 6.0), 20 mM $CaCl_2$, 5 mM $MgCl_2$, and 0.03% (w/v) *n*-dodecyl-β-D-maltoside by concentrating them to approximately 9 mg of Chl/mL with Centricon-100 concentrators (Millipore Corporation, Bedford, MA), diluting them 20-fold with a buffer containing 42% (v/v) glycerol, and then concentrating them to approximately 11 mg of Chl/mL. The concentrated samples were transferred to lucite sample holders that were designed to fit in both EPR and X-ray cryostats,[48] dark adapted for 2 h at 4 °C, and then frozen in liquid N_2. The S_2 state was generated by illuminating samples for 5 min in a nonsilvered Dewar at 198 K (dry ice/ethanol) with a focused, heat-filtered, 350-W Radiac light source. The samples were then immediately frozen in liquid nitrogen.

EPR Measurements. Continuous-wave EPR spectra were recorded with a Bruker ER 300 EPR spectrometer (Bruker BioSpin Corp., Billerica, MA) equipped with a Bruker ER 4102 ST standard cavity. The sample temperature was controlled with an Oxford ESR900 liquid helium cryostat (Oxford Instruments, Oxfordshire, U.K.). Sample manipulations were conducted under dim green light.

Measurement of Mn-XANES and Mn-EXAFS Spectra. X-ray absorption spectroscopy (XAS) was performed at the Stanford Synchrotron Radiation Laboratory (SSRL) on beamline 7-3 at an electron energy of 3.0 GeV with an average current of 300 mA. The radiation was monochromatized by a Si(220) double-crystal monochromator. The intensity of the incident X-ray beam was monitored by a N_2-filled ion chamber (I_0) in front of the sample. The monochromator energy was calibrated using a pre-edge peak of $KMnO_4$ (6543.3 eV). These standards were placed between two N_2-filled ionization chambers (I_1 and I_2) after the sample. The X-ray flux at 6.6 keV was at 1×10^{13} photons s^{-1} mm^{-2}. The monochromator was detuned at 6600 eV to 50% of maximal flux to attenuate the X-ray second harmonic. Samples were kept at a temperature of 10 K in a liquid helium flow cryostat to minimize radiation

damage. The procedures for data reduction have been described previously.[24]

Preparation of FTIR Samples. All manipulations were conducted under dim green light at 4 °C. Samples (50 μg of Chl *a*) were exchanged into FTIR analysis buffer [40 mM sucrose, 10 mM MES−NaOH (pH 6.0), 5 mM $CaCl_2$, 5 mM NaCl, 0.06% (w/v) *n*-dodecyl-β-D-maltoside[49,50]] by passage through a centrifugal gel filtration column at 27*g*.[51] They were then concentrated to 3.3 mg of Chl/mL with Amicon Ultra-0.5 mL 100 K centrifugal filter devices (EMD Millipore, Billerica, MA). Concentrated samples (6 μL in volume) were mixed with 1/10 volume of fresh 100 mM potassium ferricyanide (dissolved in water), spread to a diameter of about 13 mm in the center of a 25 × 2 mm diameter BaF_2 window, and then dried lightly (until tacky) under a stream of dry nitrogen gas. To moderately rehydrate the samples and to maintain them at 99% relative humidity in the FTIR sample compartment, four 1 μL drops of a solution of 20% (v/v) glycerol in water were spotted around the periphery of the window, not touching the sample.[52] A second BaF_2 window was placed over the first, with a 23 × 1 mm nitrile O-ring acting as a spacer. The sample assembly was sealed into an aluminum cell, loaded into a water-jacketed aluminum holder in the FTIR sample compartment, and allowed to equilibrate in darkness for 2 h. The sample was kept at a constant temperature of 0 °C by circulating a cold solution of 50% (v/v) ethylene glycol in water through the sample cell holder. Sample concentrations were adjusted so that the absolute absorbance of the amide I band at 1657 cm^{-1} was less than 1.0. For the preparation of samples having natural abundance $H_2{}^{16}O$ exchanged for $H_2{}^{18}O$, lightly dried samples were rehydrated with four 1 μL drops of a solution of 20% (v/v) glycerol in $H_2{}^{18}O$ (97% ^{18}O, Cambridge Isotope Laboratories, Inc., Andover, MA).[53]

FTIR Spectra. Midfrequency FTIR spectra were recorded with a Bruker Vertex 70 spectrometer (Bruker Optics, Billerica, MA) that was equipped with a KBr beam splitter and a preamplified, midrange D317 photovoltaic MCT detector (Kolmar Technologies, Inc., Newburyport, MA). Long-pass 2.4 μm cutoff filters (Andover Corp., Salem, NH) were mounted on both sides of the sample compartment to prevent the interferometer's coaxial helium−neon laser from illuminating the sample and to protect the MCT detector from scattered actinic illumination. Double-sided forward−backward interferograms were recorded with a scanner velocity of 120 kHz. For the calculation of Fourier transforms, a Blackman−Harris 3-term apodization function and a zero-fill factor of 2 were employed. The spectral resolution for all spectra was 4 cm^{-1}. Actinic illumination consisted of flashes (~20 mJ/flash, ~7 ns fwhm) provided by a frequency-doubled Q-switched Nd:YAG laser [BRIO (Quantel USA, Bozeman, MT)]. Flash excitation was controlled from the Vertex 70 OPUS interface. The Nd:YAG laser was programmed to deliver a single Q-switched flash during a 20 Hz flashlamp repetition series to ensure the uniformity of the laser light intensity. For each sample, after dark adaptation, six successive flashes were applied with an interval of 13 s between each (no preflashes were applied). Two single beam spectra were recorded before the first flash and one single-beam spectrum was recorded starting 0.33 s after the first and subsequent flashes (each single-beam spectrum consisted of 100 scans). The 0.33 s delay was incorporated to allow for the oxidation of Q_A^- by the ferricyanide. To obtain difference spectra corresponding to successive S-state transitions, the single-beam spectrum that was recorded after the n^{th} flash was divided by the single-beam spectrum that was recorded immediately before the n^{th} flash, and the ratio was converted to units of absorption. To estimate the background noise level, the second preflash single-beam spectrum was divided by the first and the ratio was converted to units of absorption. The sample was dark adapted for 30 min, then the cycle was repeated. The cycle was repeated 16 times for each sample, and the difference spectra recorded with several samples were averaged.

Other Procedures. Chlorophyll concentrations and initial light-saturated rates of O_2 evolution were measured as described previously.[54]

RESULTS

The light-saturated O_2 evolving activity of purified D1-E333Q PSII core complexes was 1.4 ± 0.1 mmol O_2 (mg of Chl)$^{-1}$ h^{-1} compared to 5.3 ± 0.2 mmol O_2 (mg of Chl)$^{-1}$ h^{-1} for wild-type PSII core complexes. The lower activity of the purified mutant PSII core complexes (26 ± 2% compared to that of the wild-type) correlates approximately with the lower O_2 evolving activity of D1-E333Q cells [29−36% compared to that of the wild-type[32−34]].

O_2 Flash Yields and Kinetics of O_2 Release. To further investigate the lower rates of O_2 evolution that are caused by the D1-E333Q mutation, wild-type and mutant thylakoid membranes were isolated and examined with a bare platinum electrode that permits the centrifugal deposition of samples upon the electrode surface. The pattern of O_2 yields that are produced by the individual flashes in a series of saturating single-turnover flashes provides a measure of the efficiency of the individual S-state transitions. The pattern of O_2 flash yields in D1-E333Q thylakoid membranes (Figure 2) showed the same period-four oscillations that are observed in wild-type membranes, although the amplitudes were much smaller, about 20% compared to that of the wild-type, consistent with the lower steady-state rates of O_2 evolution observed in the mutant cells and PSII core complexes. Analysis of these data revealed that the parameters that describe the factors that contribute to the damping of the oscillations (i.e., the parameters that

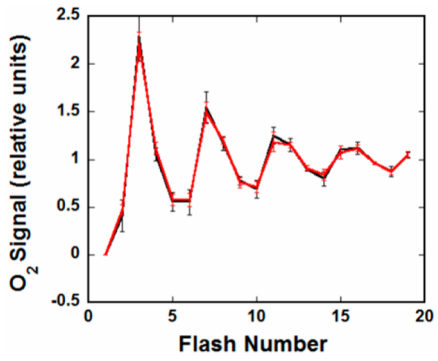

Figure 2. Comparison of the normalized flash O_2 yield patterns of wild-type (black) and D1-E333Q (red) thylakoid membranes in response to 19 saturating xenon flashes applied at a frequency of 4 Hz. Equivalent amounts of thylakoid membranes were exposed to 30 s of room light, deposited centrifugally on the surface of a bare-platinum electrode, subjected to a single preflash, and then dark adapted for ten minutes before the sequence of measuring flashes was initiated. Before normalization, the O_2 signals of the mutant thylakoid membranes were approximately 20% of that of the wild-type. Error bars represent standard deviations.

dx.doi.org/10.1021/bi401339f | *Biochemistry* 2013, 52, 8452−8464

describe misses and double hits) are virtually the same in the mutant as in the wild-type control (Table 1). This analysis also

Table 1. S-State Decay Cycling Parameters of D1-E333Q Membranes[a]

strain	S-state distribution, S_0:S_1:S_2:S_3 (%)	misses α (%)	hits β (%)	double hits γ (%)
wild-type	11:79:10:0	11	87	2
D1-E333Q	14:72:13:1	12	86	2

[a]Membranes were given a series of 20 preflashes followed by a 10 min dark-adaptation period prior to the initiation of the measuring flash sequence. Numerical analysis of the O_2 flash-yield amplitudes was performed assuming a four-state model as described previously.[45,46]

revealed that, after a 10 min period of dark adaptation, the distribution of S states in the mutant thylakoid membranes was only slightly different from that in wild-type; the percentage of PSII reaction centers in the S_1 state decreased slightly (from 79% to 72%), and the percentages in the S_0, S_2, and S_3 states increased slightly (by 3%, 3%, and 1%, respectively). The kinetics of O_2 release in D1-E333Q thylakoid membranes in comparison with those of the wild-type are presented in Figure 3. Analysis of these data showed that the kinetics of O_2 release

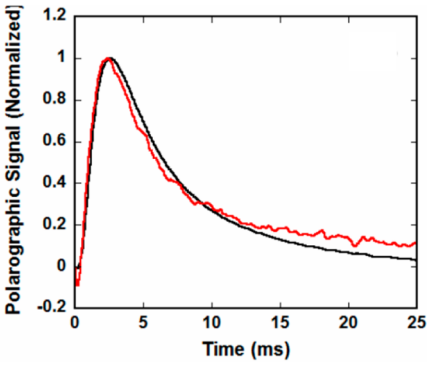

Figure 3. Comparison of the normalized flash-induced O_2 signals of wild-type (black) and D1-E333Q (red) thylakoid membranes. Equivalent amounts of thylakoid membranes were deposited centrifugally on the surface of a bare-platinum electrode and given a sequence of 120 (wild-type) or 600 (D1-E333Q) LED flashes at 4 Hz. The data show the averages from each set of kinetic traces. Before normalization, the O_2 signals of the mutant thylakoid membranes were approximately 20% of that of the wild-type.

are virtually the same in the mutant as in the wild-type, being characterized by half-times of approximately 1.2 ms.

EPR Spectra. A perpendicular polarization multiline EPR signal was observed near $g = 2$ in dark-adapted D1-E333Q PSII core complexes after illumination at 195 K (Figure 4). In terms of peak positions and spacings, this signal closely resembles the S_2 state multiline EPR signal that is observed in wild-type PSII core complexes, though with a smaller amplitude. We assign this signal to the S_2 state in the mutant. The EPR spectrum of the mutant also closely resembled that of wild-type between 500 and 2500 G (not shown). The integrated area of the six peaks indicated in the mutant S_2 state multiline EPR spectrum (asterisks on the lower trace of Figure 4) was approximately 27% of the integrated area of the corresponding peaks in the wild-type spectrum (asterisks on the upper trace of Figure 4). Accordingly, approximately 27% of the D1-E333Q PSII core

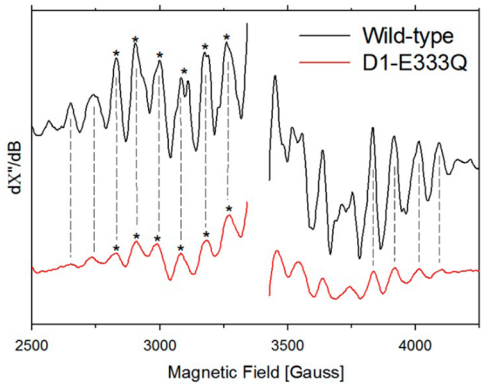

Figure 4. Comparison of the perpendicular polarization S_2 state multiline EPR signals of wild-type (black) and D1-E333Q (red) PSII core complexes. The wild-type and D1-E333Q samples contained 7.8 and 6.8 mg of Chl/mL, respectively. To correct for the lower concentration of Chl in the mutant sample, the spectrum of D1-E333Q has been multiplied vertically by a factor of 1.15. The data were recorded at 9 K with a microwave frequency of 9.48 GHz, a microwave power of 5 mW, a modulation amplitude of 32 G, a modulation frequency of 100 kHz, and a time constant of 250 ms. The wild-type and mutant spectra represent the averages of 16 and 25 scans, respectively. Each spectrum has had the large signal of $Y_D^{\bullet}$ at $g = 2$ excised for clarity. Asterisks denote peaks used to estimate the relative amplitudes of the signals (see text).

complexes were estimated to contain photooxidizable Mn_4CaO_5 clusters on the basis of the EPR data.

X-ray Absorption Data. The Mn K-edge XANES spectra of dark-adapted wild-type and D1-E333Q PSII core complexes are compared in Figure 5A. The mutant spectrum was nearly

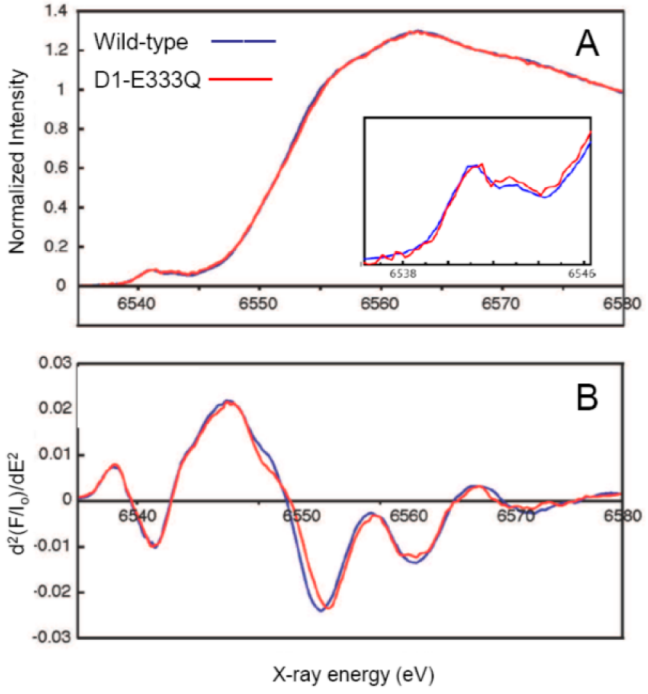

Figure 5. Comparison of the normalized Mn K-edge XANES spectra of wild-type (blue) and D1-E333Q (red) PSII core complexes poised in the S_1 state by dark adaptation. The corresponding second derivatives of the data are shown in (B). The inset in (A) shows the pre-edge region.

dx.doi.org/10.1021/bi401339f | Biochemistry 2013, 52, 8452−8464

identical to that of wild-type. The resemblance is most clearly shown by the similarity of the second derivative spectra (Figure 5B). The Mn K-edge EXAFS spectrum of dark-adapted wild-type and D1-E333Q PSII core complexes are compared in Figure 6. Again, the mutant spectrum was nearly identical to wild-type, and we assign it (and the XANES spectrum of D1-E333Q) to the S_1 state of the mutant.

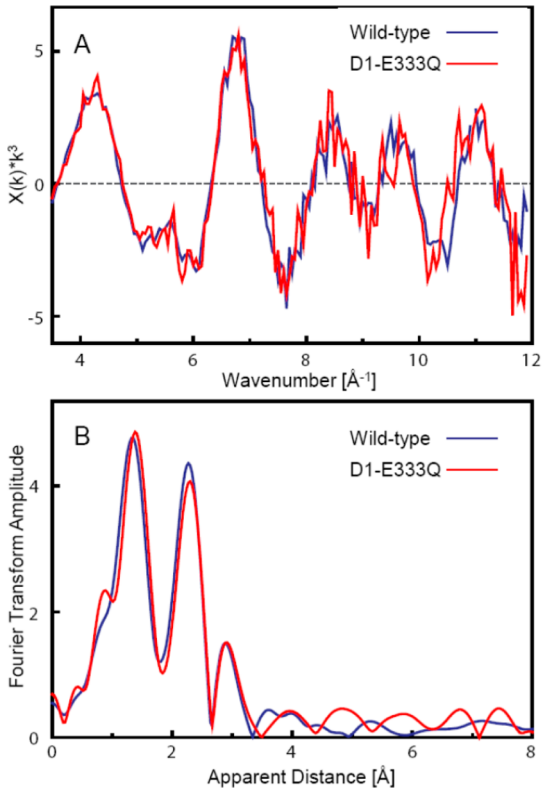

Figure 6. Comparison of the normalized k^3-space Mn-EXAFS spectra of wild-type (blue) and D1-E333Q (red) PSII core complexes poised in the S_1 state by dark adaptation (A). The Fourier transforms of the k^3-weighted Mn-EXAFS of wild-type (blue) and D1-E333Q PSII core complexes are shown (B).

FTIR Data. The FTIR difference spectra induced by four successive flashes given to D1-E333Q PSII core complexes are compared to those of the wild-type in Figure 7. The spectra that are induced by the first flash should correspond predominantly to S_2-*minus*-S_1 FTIR difference spectra.[55−58] When the overall amplitudes of the FTIR difference spectra were normalized to the amount of PSII in the sample [accomplished by normalizing the mutant and wild-type spectra to the average absolute amplitudes of the samples at the amide peak at 1657 cm^{-1}, then multiplying the amplitudes of the mutant spectra to maximize spectral overlap in the carboxylate stretching regions (by factors of 3.11 to 4.35; see the legend for Figure 7)], the amplitudes of the mutant spectra were found to be 23−32% of the amplitudes of the wild-type spectra. Accordingly, 23−32% of the D1-E333Q PSII core complexes were estimated to contain photooxidizable Mn_4CaO_5 clusters. The slightly larger bands at 1706(−) cm^{-1} and 1697(+) cm^{-1} in the D1-E333Q S_2-*minus*-S_1 FTIR difference spectrum compared to that of the wild-type probably reflect the flash-induced formation of $Y_Z^{\bullet}$ in a fraction of mutant PSII reaction centers that lack Mn_4CaO_5 clusters. However, the features of the $Y_Z^{\bullet}$-*minus*-Y_Z FTIR difference spectrum are relatively small except for positive bands at 1699, 1550, and 1512 cm^{-1}.[37,59,60] Therefore, we conclude that the first flash spectrum of D1-E333Q is dominated by the contributions of S_2-*minus*-S_1 and not by contaminating features of $Y_Z^{\bullet}$-*minus*-Y_Z.

The data of Figure 7 show that the S_{n+1}-*minus*-S_n FTIR difference spectra of D1-E333Q PSII core complexes are very similar to the corresponding spectra of wild-type PSII core complexes in the symmetric carboxylate stretching [$\nu_{sym}(COO^-)$] region and in the overlapping amide II/asymmetric carboxylate stretching [$\nu_{asym}(COO^-)$] region. In these regions, the largest changes occur in the S_2-*minus*-S_1 difference spectrum, where the positive peak at 1509 cm^{-1} upshifts to 1511 cm^{-1}, a more pronounced set of features at 1490(−)/1481(+)/1470(−) cm^{-1} appears, the small negative feature at 1452 cm^{-1} upshifts to 1454 cm^{-1}, the broad positive feature at 1438 cm^{-1} splits into positive features at 1443 and 1431 cm^{-1}, the low frequency shoulder of the negative 1400/1399 cm^{-1} feature becomes substantially more pronounced, and the positive features at 1338 and 1324 cm^{-1} are shifted slightly (to 1339 and 1322 cm^{-1}, respectively) and increased in amplitude. Other changes in these regions of the S_2-*minus*-S_1 difference spectrum are increased amplitudes of positive features at 1552 and 1530 cm^{-1} and the shifted peak at 1511 cm^{-1}, decreased amplitudes of positive features at 1635, 1622, and 1586 cm^{-1}, and increased amplitudes of negative features at 1641, 1628, and 1612 cm^{-1}. The primary changes in these regions of the other difference spectra are as follows: for the S_3-*minus*-S_2 difference spectrum, an increased amplitude of a positive feature at 1634 cm^{-1}, the appearance of a small negative feature at 1625 cm^{-1}, and a slight downshift and increased amplitude of the 1569(−)/1554(+)/1545(−) cm^{-1} feature to 1568(−)/1552(+)/1543(−) cm^{-1}; for the S_0-*minus*-S_3 difference spectrum, a shift in the negative peak at 1509 cm^{-1} to 1511 cm^{-1} (mirroring the shift in this mode during the S_2-*minus*-S_1 difference spectrum), the appearance of a small negative feature at 1644 cm^{-1}, and slightly increased amplitudes of negative features at 1623 and 1392 cm^{-1}; for the S_1-*minus*-S_0 difference spectrum, an increased amplitude of a negative feature at 1538 cm^{-1}, and new positive features at 1574 and 1543 cm^{-1}. Larger changes are observed in the amide I regions of the D1-E333Q difference spectra: the S_2-*minus*-S_1 difference spectrum showing an upshift of a positive mode from 1671 to 1674 cm^{-1} and a substantially larger 1664(−)/1651(+) cm^{-1} derivative feature; the S_3-*minus*-S_2 difference spectrum showing the appearance of a small 1704(−)/1696(+) cm^{-1} derivative feature, a small positive feature at 1677 cm^{-1}, and more intense positive features at 1667 and 1652 cm^{-1}; the S_3-*minus*-S_0 difference spectrum showing the appearance of a small positive feature at 1653 cm^{-1} and a more intense negative feature at 1672 cm^{-1}; the S_1-*minus*-S_0 difference spectrum showing the appearance of a small positive feature at 1652 cm^{-1}.

To isolate the vibrational modes in the slightly more altered S_2-*minus*-S_1 FTIR difference spectrum, and to display these alterations more clearly, the wild-type-*minus*-E333Q double difference spectrum was calculated (Figure 8). The large number of positive and negative features in this double difference spectrum show that the D1-E333Q mutation perturbs multiple carboxylate groups and peptide linkages but, importantly, shows no evidence that the mutation eliminates any specific carboxylate vibrational mode.

Of particular note, the D1-E333Q mutation does not alter the carbonyl stretching [ν(C═O)] region of any of the S_{n+1}-

dx.doi.org/10.1021/bi401339f | *Biochemistry* 2013, 52, 8452−8464

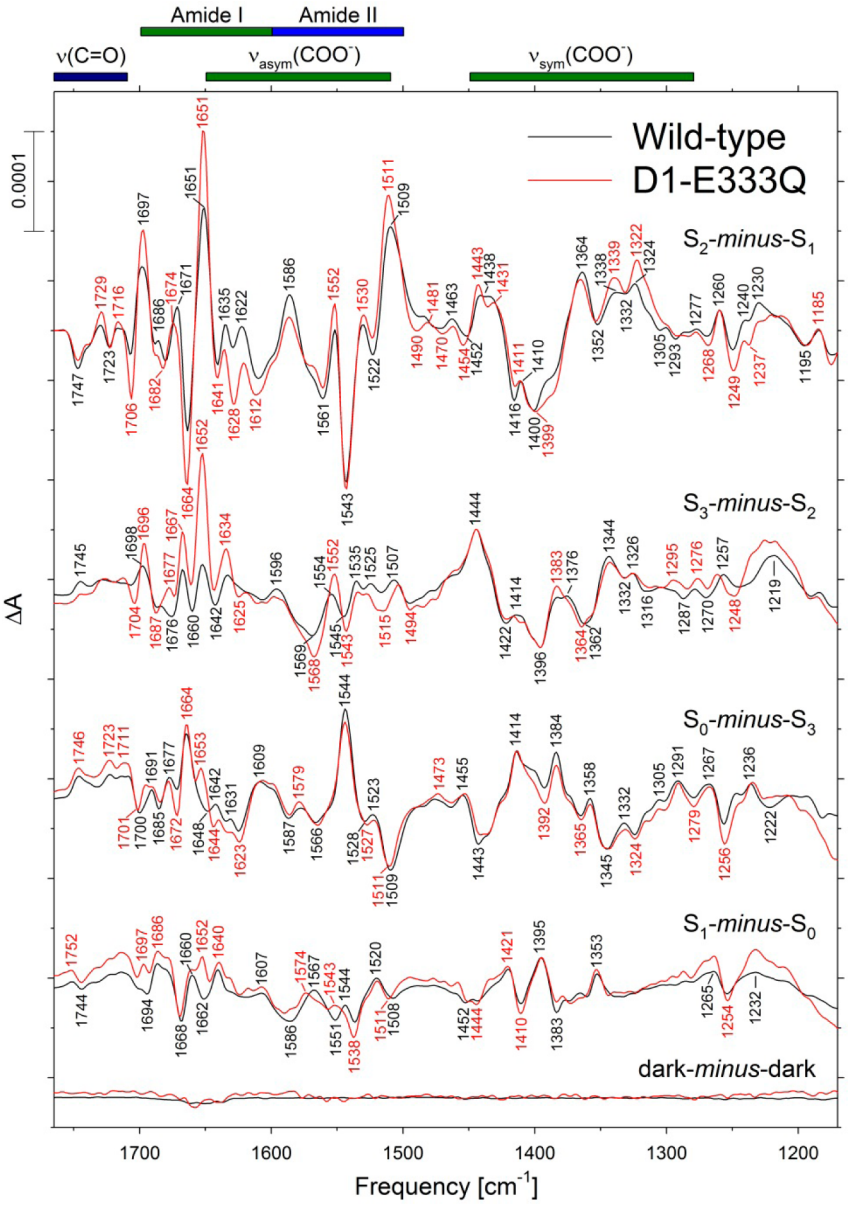

Figure 7. Comparison of the midfrequency FTIR difference spectra of wild-type (black) and D1-E333Q (red) PSII core complexes in response to four successive flash illuminations applied at 0 °C. The wild-type spectra correspond predominantly to the S_2-*minus*-S_1, S_3-*minus*-S_2, S_0-*minus*-S_3, and S_1-*minus*-S_0 FTIR difference spectra, respectively. The data (plotted from 1770 cm^{-1} to 1170 cm^{-1}) represent the averages of fourteen wild-type and fifteen D1-E333Q samples (20 400 and 22 500 scans, respectively). In order to facilitate comparisons, the mutant spectra have been multiplied vertically by factors of 3.11, 4.35, 4.14, and 4.35, respectively, after normalization to the average absolute amplitudes of the samples at the amide I peak at 1657 cm^{-1}. Dark-*minus*-dark control traces are included to show the noise level (lower traces).

minus-S_n FTIR difference spectra (see Figure 7). The amplitudes of the 1747 cm^{-1} features observed in the wild-type S_2-*minus*-S_1, S_3-*minus*-S_2, and S_0-*minus*-S_3 difference spectra are essentially unchanged by the mutation. In addition, the derivative feature observed in the wild-type S_1-*minus*-S_0 difference spectrum at 1751(+)/1744(−) cm^{-1} appears unchanged except for a 1 cm^{-1} upshift. The 1747 cm^{-1} feature corresponds to an unidentified carboxylate group whose pK_a value decreases in response to the increased charge that develops on the Mn_4Ca cluster during the S_1 to S_2 transition.[60] This group participates in a network of hydrogen bonds that extends at least 20 Å across the lumenal face of the Mn_4CaO_5 cluster and includes minimally D1-Asp61, D1-Glu65, D2-Glu312, D1-Glu329,[60] and the Cl^- ligand D2-Lys317.[25,26]

The O—H stretching vibrations of the weakly H-bonded OH groups of water molecules can be monitored between 3700 and 3500 cm^{-1}.[61−65] This region has been examined previously in PSII core complexes from *Thermosynechococcus elongatus*,[62,63] *Synechocystis sp.* PCC 6803,[66] and spinach.[67] In our wild-type *Synechocystis* PSII core complexes, this region of the S_2-*minus*-S_1 spectrum shows negative features at 3663 and 3585 cm^{-1} and a weak positive feature at 3616 cm^{-1}. The corresponding regions of the S_3-*minus*-S_2, S_0-*minus*-S_3, and S_1-*minus*-S_0 spectra show broad negative features having minima at approximately 3606, 3620, and 3619 cm^{-1}, respectively (Figure 9, black traces). The negative features in these spectra are downshifted by 930−970 cm^{-1} after exchange into D_2O (data not shown) and by 10−13 cm^{-1} after exchange into $H_2{}^{18}O$ (Figure 9, blue traces). These

dx.doi.org/10.1021/bi401339f | *Biochemistry* 2013, 52, 8452−8464

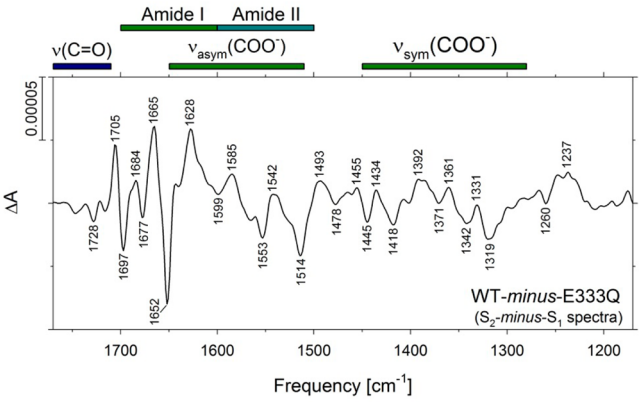

Figure 8. The double difference spectrum (wild-type-*minus*-mutant) that was obtained by subtracting the S_2-*minus*-S_1 FTIR difference spectrum of D1-E333Q from the S_2-*minus*-S_1 FTIR difference spectrum of the wild-type. The two traces shown in the top Figure 7 were subtracted directly.

isotopically induced downshifts show that these features correspond to O—H stretching vibrations.[62,63] These regions of the S_{n+1}-*minus*-S_n FTIR difference spectra of D1-E333Q PSII core complexes are compared to those of wild-type in Figure 10. This comparison shows that the D1-E333Q mutation eliminates the negative feature at 3663 cm^{-1} from the S_2-*minus*-S_1 FTIR spectrum and downshifts the broad negative feature in the S_1-*minus*-S_0 spectrum from approximately 3619 cm^{-1} to approximately 3610 cm^{-1}.

DISCUSSION

Because D1-Glu333 coordinates to a particularly dynamic region of the Mn_4CaO_5 cluster, coordinating to one Mn ion whose coordination number may change during the catalytic cycle and sharing two Mn ions with O5, an oxygen atom proposed to become incorporated into the product O_2 molecule during the final step in the catalytic cycle, it seems remarkable that any mutation constructed at D1-Glu333 would support O_2 formation. Indeed, of all the mutations constructed at D1-Glu333 (Gln, Asp, Asn, His, Cys, Ala, and Tyr), only D1-E333Q supports O_2 evolution.[32−34] Perhaps this is because Gln resembles Glu structurally. In any case, our observation that D1-E333Q thylakoid membranes evolve O_2 with normal S state parameters and release kinetics shows that, in a substantial fraction of D1-E333Q PSII reaction centers, the Mn_4CaO_5 cluster assembles and the S state transitions proceed normally. This fraction was estimated to be approximately 20% on the basis of the amplitudes of the O_2 flash yields of D1-E333Q thylakoid membranes, approximately 27% on the basis of the amplitude of the mutant S_2 state multiline EPR signal, and 23−32% on the basis of the amplitudes of the S_{n+1}-*minus*-S_n FTIR difference spectra of D1-E333Q PSII core complexes. The estimates correlate approximately with the steady-state rates of O_2 evolution observed in the mutant PSII core complexes (26 ± 2% compared to those of the wild-type), implying that those Mn_4CaO_5 clusters that assemble in the mutant are all active.

The close resemblance between our wild-type and mutant Mn-XANES and Mn-EXAFS data show that the geometric structure and electronic characteristics of the Mn_4CaO_5 cluster in the S_1 state are essentially unperturbed by the D1-E333Q mutation. The light-driven assembly of the Mn_4CaO_5 cluster involves the binding and photooxidation of a single Mn(II) ion to Mn(III) followed by protein structural rearrangements that create or increase the affinity of the binding sites for the additional Mn(II) ions and the Ca ion.[68−70] After these ions bind, the Mn ions are photooxidized to the Mn(III/IV) oxidation states characteristic of their physiological S states. The decreased yield of Mn_4CaO_5 clusters in the D1-E333Q mutant implies that D1-Glu333 plays a role in the cluster's assembly, as proposed previously.[34,68] Perhaps the D1-E333Q mutation increases the yield of inactive PSII reaction centers containing inappropriately photoligated Mn(III/IV) ions, as occurs in the *Synechocystis* mutants D1-D170H and D1-D170 V.[71] In any case, it is evident that the elimination of the negatively charged D1-Glu333 has little effect on the cluster's ability to assemble and to achieve its native conformation in a *substantial fraction* of PSII reaction centers. In contrast to D1-E333Q, the D1-H332E mutation of *Synechocystis sp.* PCC 6803 substantially alters both the geometric structure and electronic characteristics of the Mn_4CaO_5 cluster, shifting the Mn K-edge energy to a lower energy and elongating the Mn−Mn and Mn−ligand interactions to a far greater extent than are caused by any biochemical treatment (e.g., removal of Ca, exchange of Sr for Ca, or inhibition with NH_3).[72] In the case of the D1-H332E mutation, these substantial alterations were interpreted in terms of a negatively charged carboxylate oxygen replacing the τ histidyl nitrogen of D1-His332 as a ligand to a Mn(III) or Mn(IV) ion.[72] In the case of the D1-E333Q mutation, because the Mn-XANES and Mn-EXAFS data are essentially unaltered by the mutation, it is tempting to speculate that one of the carboxylate oxygens of D1-Glu333 is replaced by the carbonyl oxygen of D1-Gln333 or a water molecule and that the other is replaced by a hydroxide group.

The close resemblance of the S_2 state multiline EPR signals of wild-type and D1-E333Q PSII core complexes also shows that the mutation has little effect on the structure or electronic properties of the Mn_4CaO_5 cluster in the S_2 state. This resemblance shows that the magnetic interactions that give rise to the S_2 state multiline EPR signal[73−76] are essentially unaltered by the D1-E333Q mutation. In contrast, the *Synechocystis* D1-H332E mutation alters the electronic structure of the Mn_4CaO_5 cluster,[77] substantially altering the appearance of the S_2 state multiline EPR signal.[36,78]

Our FTIR data show that the D1-E333Q mutation causes relatively minor perturbations throughout the amide and carboxylate stretching regions of the S_{n+1}-*minus*-S_n difference spectra. These perturbations are similar in magnitude to those that have been introduced by mutations of most of the other carboxylate ligands of the Mn_4CaO_5 cluster [i.e., D1-D170H,[50,79] D1-E189Q,[51,80] D1-E189R,[51] D1-D342N,[37] and the α-COO^- group of D1-Ala344[81−84]] but are less than those introduced by the mutation CP43-E354Q.[66,85] If the vibrational modes of D1-Glu333 changed during any of the S state transitions, then replacing D1-Glu333 with Gln should eliminate the $\nu_{sym}(COO^-)$ and/or $\nu_{asym}(COO^-)$ carboxylate stretching modes of D1-Glu333 from at least one S_{n+1}-*minus*-S_n FTIR difference spectrum, possibly replacing them/it with a combination of ν(C=O) and/or $\delta(NH_2)$ modes from D1-Gln333. Such an elimination of carboxylate modes should be as obvious in the spectra as the loss of the $\nu_{asym}(COO^-)$ mode assigned to CP43-Glu354[66,85] or the [1-^{13}C]alanine-induced shift of the $\nu_{sym}(COO^-)$ mode of the α-COO^- group of D1-Ala344.[38,81,84] No such elimination is observed. Therefore, our data show that neither the symmetric nor the asymmetric carboxylate stretching mode of D1-Glu333 is altered signifi-

dx.doi.org/10.1021/bi401339f | *Biochemistry* 2013, 52, 8452−8464

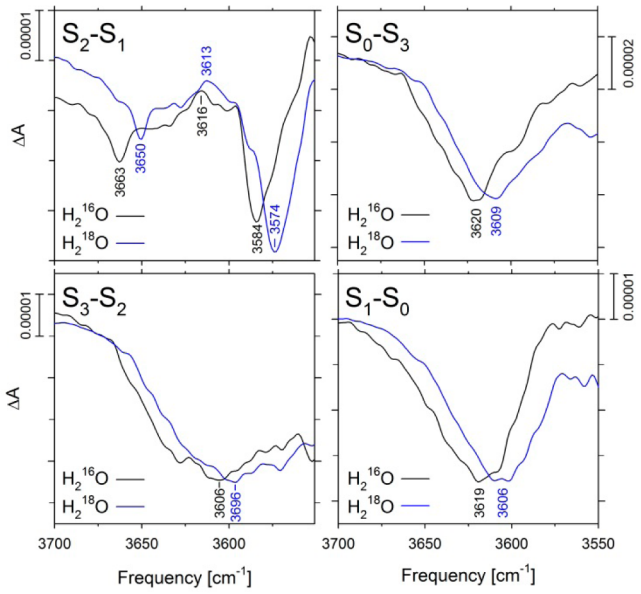

Figure 9. Comparison of the FTIR difference spectra of wild-type PSII core complexes from *Synechocystis sp.* PCC 6803 hydrated with $H_2{}^{16}O$ (black) or $H_2{}^{18}O$ (blue) in the weakly hydrogen bonded O—H stretching region in response to four successive flash illuminations applied at 0 °C. Note the different vertical scales. The $H_2{}^{16}O$ data were collected simultaneously with the data shown in Figure 7. The $H_2{}^{18}O$ data represent the averages of sixteen samples (24,100 scans) and were normalized to maximize overlap with the $H_2{}^{16}O$ data between 1800 and 1200 cm^{-1}.

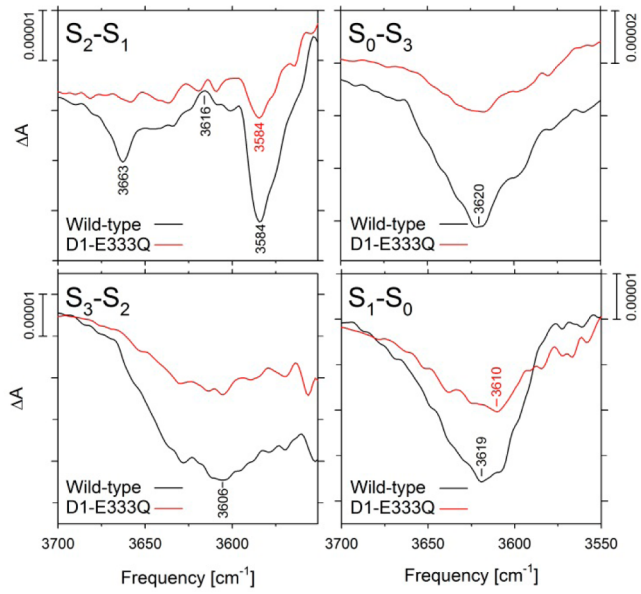

Figure 10. Comparison of the FTIR difference spectra of wild-type (black) and D1-E333Q (red) PSII core complexes in the weakly hydrogen bonded O—H stretching region in response to four successive flash illuminations applied at 0 °C. The data were collected simultaneously with data shown in Figure 7, but the mutant data were *not* multiplied vertically after normalization to the average absolute amplitudes of the samples at 1657 cm^{-1}. Note the different vertical scales.

cantly when the Mn_4CaO_5 cluster is oxidized during any of the S-state transitions. We conclude that the carboxylate group of D1-Glu333 is effectively insensitive to the oxidations of the Mn_4CaO_5 cluster and does not change its coordination mode during any of the S-state transitions. Nevertheless, the alterations that are observed in our S_{n+1}-*minus*-S_n FTIR difference spectra, particularly in the amide I regions, show that the D1-E333Q mutation slightly alters the protein's response to the charge that develops on the Mn_4CaO_5 cluster during the S_1 to S_2 transition and to the structural changes that take place during the S_2 to S_3, S_3 to S_0, and S_0 to S_1 transitions.

One of the most striking results of the FTIR studies on PSII is the insensitivity of the individual FTIR difference spectra to the mutation of four of the Mn_4Ca cluster's six carboxylate ligands. Mutations of D1-Asp170,[50,79] D1-Glu189,[51,80] D1-Asp342,[37] and D1-Glu333 (this work) fail to eliminate any carboxylate vibrational stretching modes from the S_{n+1}-*minus*-S_n FTIR difference spectra. Although some of the features in the $\nu_{sym}(COO^-)$ and $\nu_{asym}(COO^-)$ regions of the FTIR difference spectra clearly correspond to first coordination sphere ligands (i.e., CP43-Glu354 and the α-COO^- group of D1-Ala344), the majority of these features evidently correspond to residues in the cluster's second coordination sphere or beyond and reflect the response of the protein to the positive charge that develops on the Mn_4CaO_5 cluster during the S_1 to S_2 transition and to the structural changes that are associated with the S_2 to S_3, S_3 to S_0, and S_0 to S_1 transitions.

We previously provided evidence that D1-Asp61, D1-Glu65, D2-Glu312, D1-Glu329, and water molecules participate in a network of hydrogen bonds that extends at least 20 Å across the lumenal face of the Mn_4CaO_5 cluster and that this network forms part of a dominant proton egress pathway leading from the Mn_4CaO_5 cluster to the lumen.[60] This evidence was based on (i) the elimination of the same ν(C═O) mode of a protonated carboxylate group in the S_2-*minus*-S_1 FTIR difference spectrum of wild-type PSII core complexes by the mutations D1-E65A, D2-E312A, and D1-E329Q and by overdehydration of wild-type samples and (ii) on the substantial decrease in the efficiencies of the S_2 to S_3 and S_3 to S_0 transitions caused by the mutations D1-D61A, D1-E65A, and D2-E312A. The eliminated ν(C═O) mode corresponds to an unidentified carboxylate group whose pK_a value decreases in response to the increased charge that develops on the Mn_4CaO_5 cluster during the S_1 to S_2 transition. Disruption of part of this network by mutation or overdehydration prevents the transmission of the structural perturbations associated with the S_1 to S_2 transition to the unidentified carboxylate residue, thereby eliminating the pK_a change and, thereby, the ν(C═O) mode. A network of hydrogen bonds leading from the Mn_4CaO_5 cluster to the thylakoid lumen and including D1-Asp61, D1-Glu65, and D2-Glu312 can be inferred[1,86,87] from the distribution of water molecules in the 1.9 Å structural model of PSII and includes the Cl^--ligating residue D2-Lys317.[25,26] The D1-E333Q mutation does not appear to perturb this network.

Structural changes of hydrogen-bonded water molecules can be monitored by FTIR difference spectroscopy. In particular, the O—H stretching vibrations of weakly H-bonded water OH groups can be monitored between 3700 cm^{-1} and 3500 cm^{-1}, a region devoid of overlapping vibrational modes.[61−65] In PSII core complexes from *Thermosynechococcus elongatus*[62,63] and spinach,[67] this region of the S_2-*minus*-S_1 FTIR difference spectrum exhibits a derivative-shaped feature having a negative peak at 3585−3588 cm^{-1} and a positive peak at 3613−3618 cm^{-1}. This feature has been attributed to a water molecule

dx.doi.org/10.1021/bi401339f | *Biochemistry* 2013, 52, 8452−8464

coupled to the Mn_4CaO_5 cluster and having an asymmetric H-bonding structure in the S_1 state and an even greater asymmetry of H-bonding in the S_2 state.[62,63,88] The feature is substantially altered by the CP43-E354Q mutation in *Synechocystis sp.* PCC 6803.[66] Consequently, it was proposed that the water molecule whose H-bonding characteristics change during the S_1 to S_2 transition binds to one of the Mn ions that is ligated by CP43-Glu354.[66] The alterations in the 3700−3500 cm^{-1} region produced by the CP43-E354Q mutation correlate with an 8.5-fold increase in the exchange rate of W_f, the rapidly exchanging substrate water molecule.[85]

A 3622(+)/3588(−) cm^{-1} feature has been reported in the S_2-*minus*-S_1 FTIR difference spectrum of wild-type *Synechocystis sp.* PCC 6803, though the positive peak at 3622 cm^{-1} was less distinct than in *Thermosynechococcus elongatus* or spinach.[66] In our wild-type *Synechocystis* S_2-*minus*-S_1 difference spectrum (Figure 9), the negative and positive peaks appear at 3585 cm^{-1} and 3616 cm^{-1}, respectively, with the positive peak also being less distinct than in *Thermosynechococcus elongatus* or spinach. Our spectrum also contains a negative feature at 3663 cm^{-1} that has not been reported previously. Because this feature shows the same D_2O- and $H_2{}^{18}O$-induced downshifts as the other negative features in this region of the S_{n+1}-*minus*-S_n FTIR difference spectra, we conclude that this feature also arises from a weakly H-bonded OH group. That the 3663 cm^{-1} feature has not been reported previously might be attributed to the higher hydration of our samples compared to those examined previously. The extent of sample hydration is known to substantially affect the amplitudes of features in the S_{n+1}-*minus*-S_n FTIR difference spectra.[25,52,60]

The S_3-*minus*-S_2, S_0-*minus*-S_3, and S_1-*minus*-S_0 FTIR difference spectra of PSII from *Thermosynechococcus elongatus* exhibit broad negative features having minima at 3634, 3621, and 3612 cm^{-1}, respectively.[63] These features have been attributed to water molecules or hydroxide groups that are located on or near the Mn_4CaO_5 cluster and that either deprotonate or form stronger hydrogen bonds (i.e., weakly H-bonded OH groups become strongly H-bonded) during the S_2 to S_3, S_3 to S_0, and S_0 to S_1 transitions.[63,88] Accordingly, we assign the negative feature at 3663 cm^{-1} observed in our wild-type S_2-*minus*-S_1 FTIR difference spectrum to a water molecule or hydroxide group on or near the Mn_4CaO_5 cluster that either deprotonates or forms a stronger hydrogen bond during the S_1 to S_2 transition. Because the feature is eliminated by the D1-E333Q mutation, we conclude that the H-bonding properties of this water molecule or hydroxide group are altered by the mutation.

In our spectra of wild-type *Synechocystis sp.* PCC 6803, the S_3-*minus*-S_2, S_0-*minus*-S_3, and S_1-*minus*-S_0 spectra exhibit broad negative features having minima at approximately 3606, 3620, and 3619 cm^{-1}, respectively. The minima in the S_3-*minus*-S_2 and S_1-*minus*-S_0 spectra are shifted from those observed with *Thermosynechococcus elongatus*, particularly the minimum in the S_3-*minus*-S_2 spectrum. These shifts may reflect slight differences between the networks of hydrogen bonds around the Mn_4CaO_5 cluster in the two species of cyanobacteria. Because the D1-E333Q mutation causes an approximately 9 cm^{-1} downshift of the negative feature in the S_1-*minus*-S_0 FTIR difference spectrum, we conclude that the D1-E333Q mutation also alters the hydrogen-bonding properties of a water molecule or hydroxide group that is located on or near the Mn_4CaO_5 cluster and that either deprotonates or forms a stronger hydrogen bond during the S_0 to S_1 transition.

SUMMARY AND CONCLUSIONS

The D1-E333Q mutation decreases the yield of assembled Mn_4CaO_5 clusters, implying that this residue plays a role in the cluster's assembly. Nevertheless, the Mn_4CaO_5 clusters that assemble in the presence of the D1-E333Q mutation function normally as shown by O_2 flash yields, O_2 release kinetics, EPR spectroscopy, Mn-XANES and Mn-EXAFS measurements, and FTIR difference spectroscopy. Because the D1-E333Q mutation eliminates or shifts features in the weakly H-bonded O—H stretching regions of the S_2-*minus*-S_1 and S_1-*minus*-S_0 FTIR difference spectra, we conclude that the mutation alters the H-bonding properties of one or more water molecules or hydroxide groups that are located on or near the Mn_4CaO_5 cluster and that either deprotonate or form stronger hydrogen bonds during the S_0 to S_1 and S_1 to S_2 transitions.

AUTHOR INFORMATION

Corresponding Author

*R. J. Debus. E-mail: richard.debus@ucr.edu. Phone: (951) 827-3483. Fax: (951) 827-4294.

Present Addresses

[⊥]Zilkha Neurogenetic Institute, University of Southern California, Los Angeles, California 90093, United States
[#]Department of Chemistry, Washington University, St. Louis, Missouri 63130, United States

Funding

Mutant construction, EPR measurements, and FTIR studies were supported by the Department of Energy, Office of Basic Energy Sciences, Division of Chemical Sciences (grant DE-FG02-10ER16191 to R.J.D.), X-ray absorption studies were supported by the Department of Energy, Office of Basic Energy Sciences, Division of Chemical Sciences (grant DE-AC02-05CH11231 to J.Y.), oxygen release studies were supported by the National Science Foundation (grant MCB-1244586 to R.L.B.)

Notes

The authors declare no competing financial interest.

ACKNOWLEDGMENTS

The authors are grateful to Anh P. Nguyen for maintaining the mutant and wild-type cultures of *Synechocystis sp.* PCC 6803 and for purifying the thylakoid membranes that were used for measurements and the isolation of PSII core complexes and to Dimitri Niks for assistance with collecting the EPR data.

ABBREVIATIONS

Chl, chlorophyll; DCMU, 3-(3,4-dichlorophenyl)-1,1-dimethylurea; EDTA, ethylenediaminetetraacetic acid; EPR, electron paramagnetic resonance; EXAFS, extended X-ray absorption fine structure; FTIR, Fourier transform infrared; LED, light-emitting diode; MES, 2-(*N*-morpholino)ethanesulfonic acid; NTA, nitrilotriacetic acid; P_{680}, chlorophyll multimer that serves as the light-induced electron donor in PSII; Pheo, pheophytin; PSII, photosystem II; Q_A, primary plastoquinone electron acceptor; Q_B, secondary plastoquinone electron acceptor; XANES, X-ray absorption near edge structure; Y_Z, tyrosine residue that mediates electron transfer between the Mn_4Ca cluster and $P_{680}{}^{+\bullet}$; Y_D, second tyrosine residue that can reduce $P_{680}{}^{+\bullet}$ in PSII

REFERENCES

(1) Umena, Y., Kawakami, K., Shen, J.-R., and Kamiya, N. (2011) Crystal Structure of Oxygen-Evolving Photosystem II at a Resolution of 1.9 Å. *Nature 473*, 55−60.

(2) Cardona, T., Sedoud, A., Cox, N., and Rutherford, A. W. (2012) Charge separation in Photosystem II: A comparative and evolutionary overview. *Biochim. Biophys. Acta 1817*, 26−43.

(3) Barber, J. (2012) Photosystem II: The Water-Splitting Enzyme of Photosynthesis, Cold Spring Harbor Symp. *Quant. Biol. 77*, 295−307.

(4) Shi, L.-X., Hall, M., Funk, C., and Schröder, W. P. (2012) Photosystem II, a growing complex: Updates on newly discovered components and low molecular mass proteins. *Biochim. Biophys. Acta 1817*, 13−25.

(5) Messinger, J., Noguchi, T., and Yano, J. (2012) Photosynthetic O_2 Evolution, in *Molecular Solar Fuels* (Wydrzynski, T. and Hillier, W., Eds.) pp 163−207, Royal Society of Chemistry, Cambridge, UK.

(6) Renger, G. (2012) Mechanism of light induced water splitting in Photosystem II of oxygen evolving photosynthetic organisms. *Biochim. Biophys. Acta 1817*, 1164−1176.

(7) Dau, H., Zaharieva, I., and Haumann, M. (2012) Recent developments in research on water oxidation by photosystem II. *Curr. Opin. Chem. Biol. 16*, 3−10.

(8) Cox, N., Pantazis, D. A., Neese, F., and Lubitz, W. (2013) Biological Water Oxidation. *Acc. Chem. Res. 46*, 1588−1596.

(9) Cox, N., and Messinger, J. (2013) Reflections on substrate water and dioxygen formation. *Biochim. Biophys. Acta 1827*, 1020−1030.

(10) Kawakami, K., Umena, Y., Kamiya, N., and Shen, J.-R. (2011) Structure of the Catalytic, Inorganic Core of Oxygen-Evolving Photosystem II at 1.9 Å Resolution. *J. Photochem. Photobiol., B: Biol. 104*, 9−18.

(11) Luber, S., Rivalta, I., Umena, Y., Kawakami, K., Shen, J.-R., Kamiya, N., Brudvig, G. W., and Batista, V. S. (2011) S_1-State Model of the O_2-Evolving Complex of Photosystem II. *Biochemistry 50*, 6308−6311.

(12) Ames, W., Pantazis, D. A., Krewald, V., Cox, N., Messinger, J., Lubitz, W., and Neese, F. (2011) Theoretical Evaluation of Structural Models of the S2 State in the Oxygen Evolving Complex of Photosystem II: Protonation States and Magnetic Interactions. *J. Am. Chem. Soc. 133*, 19743−19757.

(13) Siegbahn, P. E. M. (2011) The Effect of Backbone Constraints: The Case of Water Oxidation by the Oxygen-Evolving Complex in PSII. *ChemPhysChem 12*, 3274−3280.

(14) Kusunoki, M. (2011) S_1-state Mn_4Ca complex of Photosystem II exists in equilibrium between the two most-stable isomeric substates: XRD and EXAFS evidence. *J. Photochem. Photobiol., B: Biol. 104*, 100−110.

(15) Galstyan, A., Robertazzi, A., and Knapp, E. W. (2012) Oxygen-Evolving Mn Cluster in Photosystem II: The Protonation Pattern and Oxidation State in the High-Resolution Crystal Structure. *J. Am. Chem. Soc. 134*, 7442−7449.

(16) Isobe, H., Shoji, M., Yamanaka, S., Umena, Y., Kawakami, K., Kamiya, N., Shen, J.-R., and Yamaguchi, K. (2012) Theoretical illumination of water-inserted structures of the $CaMn_4O_5$ cluster in the S_2 and S_3 states of oxygen-evolving complex of photosystem II: full geometry optimizations by B3LYP hybrid density functional. *Dalton Trans. 41*, 13727−13740.

(17) Siegbahn, P. E. M. (2009) Structures and Energetics for O_2 Formation in Photosystem II. *Acc. Chem. Res. 42*, 1871−1880.

(18) Yamanaka, S., Isobe, H., Kanda, K., Saito, T., Umena, Y., Kawakami, K., Shen, J.-R., Kamiya, N., Okamura, M., Nakamura, H., and Yamaguchi, K. (2011) Possible mechanisms for the O-O bond formation in oxygen evolution reaction at the $CaMn_4O_5(H_2O)_4$ cluster of PSII refined to 1.9 Å resolution. *Chem. Phys. Lett. 511*, 138−145.

(19) Siegbahn, P. E. M. (2012) Mechanisms for proton release during water oxidation in the S_2 to S_3 and S_3 to S_4 transitions in photosystem II. *Phys. Chem. Chem. Phys. 14*, 4849−4856.

(20) Rapatskiy, L., Cox, N., Savitsky, A., Ames, W. M., Sander, J., Nowaczyk, M. M., Rögner, M., Boussac, A., Neese, F., Messinger, J., and Lubitz, W. (2012) Detection of Water-Binding Sites of the Oxgyen-Evolving Complex of Photosystem II Using W-band ^{17}O Electron-Electron Double Resonance-Detected NMR Spectroscopy. *J. Am. Chem. Soc. 134*, 16619−16634.

(21) Siegbahn, P. E. M. (2013) Water oxidation mechanism in photosystem II, including oxidations, proton release pathways, O-O bond formation and O_2 release. *Biochim. Biophys. Acta 1827*, 1003−1019.

(22) Navarro, M. P., Ames, W. M., Nilsson, H., Lohmiller, T., Pantazis, D. A., Rapatskiy, L., Nowaczyk, M. M., Neese, F., Boussac, A., Messinger, J., Lubitz, W., and Cox, N. (2013) Ammonia binding to the oxygen-evolving complex of photosystem II identified the solvent-exchangeable oxygen bridge (μ-oxo) of the manganese tetramer. *Proc. Natl. Acad. Sci. U. S. A. 110*, 15561−15566.

(23) Pantazis, D. A., Ames, W., Cox, N., Lubitz, W., and Neese, F. (2012) Two Interconvertable Structures that Explain the Spectroscopic Properties of the Oxygen-Evolving Complex of Photosystem II in the S_2 State. *Angew. Chem., Int. Ed. 51*, 9935−9940.

(24) Glöckner, C., Kern, J., Broser, M., Zouni, A., Yachandra, V. K., and Yano, J. (2013) Structural Changes of the Oxygen-evolving Complex in Photosystem II during the Catalytic Cycle. *J. Biol. Chem. 288*, 22607−22620.

(25) Suzuki, H., Yu, J., Kobayashi, T., Nakanishi, H., Nixon, P. J., and Noguchi, T. (2013) Functional Roles of D2-Lys317 and the Interacting Chloride Ion in the Water Oxidation Reaction of Photosystem II As Revealed by Fourier Transform Infrared Analysis. *Biochemistry 52*, 4748−4757.

(26) Pokhrel, R., Service, R. J., Debus, R. J., and Brudvig, G. W. (2013) Mutation of Lysine 317 in the D2 Subunit of Photosystem II Alters Chloride Binding and Proton Transport. *Biochemistry 52*, 4758−4773.

(27) McEvoy, J. P., and Brudvig, G. W. (2006) Water-Splitting Chemistry of Photosystem II. *Chem. Rev. 106*, 4455−4483.

(28) Dau, H., and Haumann, M. (2007) Eight steps preceding O-O bond formation in oxygenic photosynthesis — A basis reaction cycle of the Photosystem II manganese complex. *Biochim. Biophys. Acta 1767*, 472−483.

(29) Dau, H., and Haumann, M. (2008) The Manganese Complex of Photosystem II in its Reaction Cycle — Basic Framework and Possible Realization at the Atomic Level. *Coord. Chem. Rev. 252*, 273−295.

(30) Sproviero, E. M., Gascón, J. A., McEvoy, J. P., Brudvig, G. W., and Batista, V. S. (2008) Quantum Mechanics/Molecular Mechanics Study of the Catalytic Cycle of Water Splitting In Photosystem II. *J. Am. Chem. Soc. 130*, 3428−3442.

(31) Dau, H., Limberg, C., Reier, T., Risch, M., Roggan, S., and Strasser, P. (2010) The Mechanism of Water Oxidation: From Electrolysis via Homogeneous to Biological Catalysis. *ChemCatChem 2*, 724−761.

(32) Nixon, P. J., and Diner, B. A. (1994) Analysis of Water-Oxidation Mutants Constructed in the Cyanobacterium *Synechocystis* sp. PCC 6803. *Biochem. Soc. Trans. 22*, 338−343.

(33) Chu, H.-A., Nguyen, A. P., and Debus, R. J. (1995) Amino Acid Residues that Influence the Binding of Manganese or Calcium to Photosystem II. 2. The Carboxy-terminal Domain of the D1 Polypeptide. *Biochemistry 34*, 5859−5882.

(34) Cohen, R. O., Nixon, P. J., and Diner, B. A. (2007) Participation of the C-terminal Region of the D1-Polypeptide in the First Steps in the Assembly of the Mn_4Ca Cluser of Photosystem II. *J. Biol. Chem. 282*, 7209−7218.

(35) Chu, H.-A., Nguyen, A. P., and Debus, R. J. (1994) Site-Directed Photosystem II Mutants with Perturbed Oxygen Evolving Properties: 1. Instability or Inefficient Assembly of the Manganese Cluster In Vivo. *Biochemistry 33*, 6137−6149.

(36) Debus, R. J., Campbell, K. A., Gregor, W., Li, Z.-L., Burnap, R. L., and Britt, R. D. (2001) Does Histidine 332 of the D1 Polypeptide Ligate the Manganese Cluster in Photosystem II? An Electron Spin Echo Envelope Modulation Study. *Biochemistry 40*, 3690−3699.

(37) Strickler, M. A., Walker, L. M., Hillier, W., Britt, R. D., and Debus, R. J. (2007) No Evidence from FTIR Difference Spectroscopy That Aspartate-342 of the D1 Polypeptide Ligates a Mn Ion That

Undergoes Oxidation during the S_0 to S_1, S_1 to S_2, or S_2 to S_3 Transitions in Photosystem II. *Biochemistry 46*, 3151−3160.
(38) Strickler, M. A., Walker, L. M., Hillier, W., and Debus, R. J. (2005) Evidence from Biosynthetically Incorporated Strontium and FTIR Difference Spectroscopy that the C-Terminus of the D1 Polypeptide of Photosystem II Does Not Ligate Calcium. *Biochemistry 44*, 8571−8577.
(39) Tang, X.-S., and Diner, B. A. (1994) Biochemical and Spectroscopic Characterization of a New Oxygen-Evolving Photosystem II Core Complex from the Cyanobacterium *Synechocystis* sp. PCC 6803. *Biochemistry 33*, 4594−4603.
(40) Boussac, A., Rappaport, F., Carrier, P., Verbavatz, J.-M., Gobin, R., Kirilovsky, D., Rutherford, A. W., and Sugiura, M. (2004) Biosynthetic Ca^{2+}/Sr^{2+} Exchange in the Photosystem II Oxygen-Evolving Enzyme of *Thermosynechococcus elongatus*. *J. Biol. Chem. 279*, 22809−22819.
(41) Lakshmi, K. V., Reifler, M. J., Chisholm, D. A., Wang, J. Y., Diner, B. A., and Brudvig, G. W. (2002) Correlation of the cytochrome c_{550} content of cyanobacterial Photosystem II with the EPR properties of the oxygen-evolving complex. *Photosynth. Res. 72*, 175−189.
(42) Burnap, R. L., Qian, M., and Pierce, C. (1996) The Manganese-Stabilizing Protein of Photosystem II Modifies the *in vivo* Deactivation Kinetics of the H_2O Oxidation Complex in *Synechocystis* sp. PCC 6803. *Biochemistry 35*, 874−882.
(43) Qian, M., Dao, L., Debus, R. J., and Burnap, R. L. (1999) Impact of Mutations within the Putative Ca^{2+}-Binding Lumenal Interhelical a-b Loop of the Photosystem II D1 Protein on the Kinetics of Photoactivation and H_2O-Oxidation in *Synechocystis* sp. PCC 6803. *Biochemistry 38*, 6070−6081.
(44) Dilbeck, D. L., Hwang, H. J., Zaharieva, I., Gerencser, L., Dau, H., and Burnap, R. L. (2012) The D1-D61N Mutation in *Synechocystis* sp. PCC 6803 Allows the Observation of pH-Sensitive Intermediates in the Formation and Release of O_2 from Photosystem II. *Biochemistry 51*, 1079−1091.
(45) Lavorel, J. (1976) Matrix Analysis of the Oxygen Evolving System of Photosynthesis. *J. Theor. Biol. 57*, 171−185.
(46) Meunier, P. C., Burnap, R. L., and Sherman, L. A. (1996) Improved 5-step Modeling of the Photosystem II S-state Mechanism in Cyanobacteria. *Photosynth. Res. 47*, 61−76.
(47) Jursinic, P. A., and Dennenberg, R. J. (1990) Oxygen Release Time in Leaf Discs and Thylakoids of Peas and Photosystem II Membrane Fragments of Spinach. *Biochim. Biophys. Acta 1020*, 195−206.
(48) Yano, J., Pushkar, Y., Glatzel, P., Lewis, A., Sauer, K., Messinger, J., Bergmann, U., and Yachandra, V. K. (2005) High-Resolution Mn EXAFS of the Oxygen-Evovling Complex in Photosystem II: Structural Implications for the Mn_4Ca Cluster. *J. Am. Chem. Soc.*, 14974−14975.
(49) Yamanari, T., Kimura, Y., Mizusawa, N., Ishii, A., and Ono, T.-A. (2004) Mid- to Low-Frequency Fourier Transform Infrared Spectra of S-State Cycle for Photosynthetic Water Oxidation in *Synechocystis* sp. PCC 6803. *Biochemistry 43*, 7479−7490.
(50) Debus, R. J., Strickler, M. A., Walker, L. M., and Hillier, W. (2005) No Evidence from FTIR Difference Spectroscopy That Aspartate-170 of the D1 Polypeptide Ligates a Manganese Ion That Undergoes Oxidation during the S_0 to S_1, S_1 to S_2, or S_2 to S_3 Transitions in Photosystem II. *Biochemistry 44*, 1367−1374.
(51) Strickler, M. A., Hillier, W., and Debus, R. J. (2006) No Evidence from FTIR Difference Spectroscopy that Glutamate-189 of the D1 Polypeptide Ligates a Mn Ion that Undergoes Oxidation During the S_0 to S_1, S_1 to S_2, or S_2 to S_3 Transitions in Photosystem II. *Biochemistry 45*, 8801−8811.
(52) Noguchi, T., and Sugiura, M. (2002) Flash-Induced FTIR Difference Spectra of the Water Oxidizing Complex in Moderately Hydrated Photosystem II Core Films: Effect of Hydration Extent on S-State Transitions. *Biochemistry 41*, 2322−2330.
(53) Suzuki, H., Sugiura, M., and Noguchi, T. (2008) Monitoring Water Reactions during the S-State Cycle of the Photosynthetic Water-Oxidizing Center: Detection of the DOD Bending Vibrations by Means of Fourier Transform Infrared Spectroscopy. *Biochemistry 47*, 11024−11030.
(54) Hays, A.-M. A., Vassiliev, I. R., Golbeck, J. H., and Debus, R. J. (1998) Role of D1-His190 in Proton-Coupled Electron Transfer Reactions in Photosystem II: A Chemical Complementation Study. *Biochemistry 37*, 11352−11365.
(55) Chu, H.-A., Hillier, W., Law, N. A., and Babcock, G. T. (2001) Vibrational Spectroscopy of the Oxygen-Evolving Complex and of Manganese Model Compounds. *Biochim. Biophys. Acta 1503*, 69−82.
(56) Noguchi, T. and Berthomieu, C. (2005) Molecular Analysis by Vibrational Spectroscopy, in *Photosystem II: The Light-Driven Water:-Plastoquinone Oxidoreductase* (Wydrzynski, T. and Satoh, Ki., Eds.) pp 367−387, Springer, Dordrecht, The Netherlands.
(57) Noguchi, T. (2007) Light-Induced FTIR Difference Spectroscopy as a Powerful Tool Toward Understanding the Molecular Mechanism of Photosynthetic Oxygen Evolution. *Photosynth. Res. 91*, 59−69.
(58) Noguchi, T. (2008) Fourier Transform Infrared Analysis of the Photosynthetic Oxygen-Evolving Center. *Coord. Chem. Rev. 251*, 336−346.
(59) Berthomieu, C., Hienerwadel, R., Boussac, A., Breton, J., and Diner, B. A. (1998) Hydrogen-Bonding of Redox-Active Tyrosine Z of Photosystem II Probed by FTIR Difference Spectroscopy. *Biochemistry 37*, 10547−10554.
(60) Service, R. J., Hillier, W., and Debus, R. J. (2010) Evidence from FTIR Difference Spectroscopy of an Extensive Network of Hydrogen Bonds near the Oxygen-Evolving Mn_4Ca Cluster of Photosystem II Involving D1-Glu65, D2-Glu312, and D1-Glu329. *Biochemistry 49*, 6655−6669.
(61) Kandori, H. (2000) Role of internal water molecules in bacteriorhodopsin. *Biochim. Biophys. Acta 1460*, 177−191.
(62) Noguchi, T., and Sugiura, M. (2000) Structure of an Active Water Molecule in the Water-Oxidizing Complex of Photosystem II as Studied by FTIR Spectroscopy. *Biochemistry 39*, 10943−10949.
(63) Noguchi, T., and Sugiura, M. (2002) FTIR Detection of Water Reactions During the Flash-Induced S-State Cycle of the Photosynthetic Water-Oxidizing Complex. *Biochemistry 41*, 15706−15712.
(64) Garczarek, F., and Gerwert, K. (2006) Functional waters in intraprotein proton transfer monitored by FTIR difference spectroscopy. *Nature 439*, 109−112.
(65) Maréchal, A., and Rich, P. R. (2011) Water molecule reorganization in cytochrome *c* oxidase revealed by FTIR spectroscopy. *Proc. Natl. Acad. Sci. U. S. A. 108*, 8634−8638.
(66) Shimada, Y., Suzuki, H., Tsuchiya, T., Tomo, T., Noguchi, T., and Mimuro, M. (2009) Effect of a Single-Amino Acid Substitution of the 43 kDa Chlorophyll Protein on the Oxygen-Evolving Reaction of the Cyanobacterium *Synechocystis* sp. PCC 6803: Analysis of the Glu354Gln Mutation. *Biochemistry 48*, 6095−6103.
(67) Hou, L.-H., Wu, C.-M., Huang, H.-H., and Chu, H.-A. (2011) Effects of Ammonia on the Structure of the Oxygen-Evolving Complex in Photosystem II As Revealed by Light-Induced FTIR Difference Spectroscopy. *Biochemistry 50*, 9248−9254.
(68) Burnap, R. L. (2004) D1 Protein Processing and Mn Cluster Assembly in Light of the Emerging Photosystem II Structure. *Phys. Chem. Chem. Phys. 6*, 4803−4809.
(69) DasGupta, J., Ananyev, G. M., and Dismukes, G. C. (2008) Photoassembly of the Water-Oxidizing Complex in Photosystem II. *Coord. Chem. Rev. 252*, 347−360.
(70) Becker, K., Cormann, K. U., and Nowaczyk, M. M. (2011) Assembly of the Water-Oxidizing Complex in Photosystem II. *J. Photochem. Photobiol., B: Biol. 104*, 204−211.
(71) Hwang, H. J., McLain, A., Debus, R. J., and Burnap, R. L. (2007) Photoassembly of the Manganese Cluster in Mutants Perturbed in the High Affinity Mn-Binding Site of the H_2O-Oxidation Complex of Photosystem II. *Biochemistry 46*, 13648−13657.
(72) Yano, J., Walker, L. M., Strickler, M. A., Service, R. J., Yachandra, V. K., and Debus, R. J. (2011) Altered Structure of the Mn_4Ca Cluster in the Oxygen Evolving Complex of Photosystem II by a Histidine Ligand Mutation. *J. Biol. Chem. 286*, 9257−9267.

(73) Peloquin, J. M., Campbell, K. A., Randall, D. W., Evanchik, M. A., Pecoraro, V. L., Armstrong, W. H., and Britt, R. D. (2000) ^{55}Mn ENDOR of the S_2-state Multiline EPR Signal of Photosystem II: Implications on the Structure of the Tetranuclear Mn Cluster. *J. Am. Chem. Soc. 122*, 10926−10942.
(74) Kulik, L., Epel, B., Lubitz, W., and Messinger, J. (2007) Electronic Structure of the Mn_4O_xCa Cluster in the S_0 and S_2 States of the Oxygen-Evolving Complex of Photosystem II Based on Pulse ^{55}Mn-ENDOR and EPR Spectroscopy. *J. Am. Chem. Soc. 129*, 13421−13435.
(75) Cox, N., Rapatskiy, L., Su, J.-H., Pantazis, D. A., Sugiura, M., Kulik, L., Dorlet, P., Rutherford, A. W., Neese, F., Boussac, A., Lubitz, W., and Messinger, J. (2011) Effect of Ca^{2+}/Sr^{2+} Substitution on the Electronic Structure of hte Oxygen-Evolving Complex of Photosystem II: A Combined Multifrequency EPR, ^{55}Mn-ENDOR, and DFT Study of the S_2 State. *J. Am. Chem. Soc. 133*, 3635−3648 (Correction pg. 14149).
(76) Su, J.-H., Cox, N., Ames, W., Pantazis, D. A., Rapatskiy, L., Lohmiller, T., Kulik, L. V., Dorlet, P., Rutherford, A. W., Neese, F., Boussac, A., Lubitz, W., and Messinger, J. (2011) The electronic structures of the S_2 states of the oxygen-evolving complexes of photosystem II in plants and cyanobacteria in the presence and absence of methanol. *Biochim. Biophys. Acta 1807*, 829−840.
(77) Stich, T. A., Yeagle, G. J., Service, R. J., Debus, R. J., and Britt, R. D. (2011) Ligation of D1-His332 and D1-Asp170 to the Manganese Cluster of Photosystem II from *Synechocystis* Assessed by Multi-frequency Pulse EPR Spectroscopy. *Biochemistry 50*, 7390−7404.
(78) Debus, R. J., Campbell, K. A., Peloquin, J. M., Pham, D. P., and Britt, R. D. (2000) Histidine 332 of the D1 Polypeptide Modulates the Magnetic and Redox Properties of the Manganese Cluster and Tyrosine Y_Z in Photosystem II. *Biochemistry 39*, 470−478.
(79) Chu, H.-A., Debus, R. J., and Babcock, G. T. (2001) D1-Asp170 is Structurally Coupled to the Oxygen Evolving Complex in Photosystem II as Revealed by Light-Induced Fourier Transform Infrared Difference Spectroscopy. *Biochemistry 40*, 2312−2316.
(80) Kimura, Y., Mizusawa, N., Ishii, A., Nakazawa, S., and Ono, T.-A. (2005) Changes in Structural and Functional Properties of Oxygen-Evolving Complex Induced by Replacement of D1-Glutamate 189 with Glutamine in Photosystem II: Ligation of Glutamate 189 Carboxylate to the Manganese Cluster. *J. Biol. Chem. 280*, 37895−37900.
(81) Chu, H.-A., Hillier, W., and Debus, R. J. (2004) Evidence that the C-Terminus of the D1 Polypeptide is Ligated to the Manganese Ion that Undergoes Oxidation During the S_1 to S_2 Transition: An Isotope-Edited FTIR Study. *Biochemistry 43*, 3152−3166.
(82) Mizusawa, N., Kimura, Y., Ishii, A., Yamanari, T., Nakazawa, S., Teramoto, H., and Ono, T.-A. (2004) Impact of Replacement of D1 C-terminal Alanine with Glycine on Structure and Function of Photosynthetic Oxygen-Evolving Complex. *J. Biol. Chem. 279*, 29622−29627.
(83) Mizusawa, N., Yamanari, T., Kimura, Y., Ishii, A., Nakazawa, S., and Ono, T.-A. (2004) Changes in the Functional and Structural Properties of the Mn Cluster Induced by Replacing the Side Group of the C-Terminus of the D1 Protein of Photosystem II. *Biochemistry 43*, 14644−14652.
(84) Kimura, Y., Mizusawa, N., Yamanari, T., Ishii, A., and Ono, T.-A. (2005) Structural Changes of D1 C-terminal α-Carboxylate during S-state Cycling of Photosynthetic Oxygen Evolution. *J. Biol. Chem. 280*, 2078−2083.
(85) Service, R. J., Yano, J., McConnell, I., Hwang, H. J., Niks, D., Hille, R., Wydrzynski, T., Burnap, R. L., Hillier, W., and Debus, R. J. (2011) Participation of Glutamate-354 of the CP43 Polypeptide in the Ligation of Manganese and the Binding of Substrate Water in Photosystem II. *Biochemistry 50*, 63−81.
(86) Bondar, A.-N., and Dau, H. (2012) Exptended protein/water H-bond networks in photosynthetic water oxidation. *Biochim. Biophys. Acta 1817*, 1177−1190.
(87) Linke, K., and Ho, F. M. (2013) Water in Photosystem II: Structural, functional, and mechanistic considerations. *Biochim. Biophys. Acta 1837*, 14−32.
(88) Noguchi, T. (2007) FTIR Detection of Water Reactions in the Oxygen-Evolving Center of Photosystem II. *Philos. Trans. R. Soc. London, Ser. B 363*, 1189−1195.